Research Article

Feng Ji, Yuchuan Shi*, Lei Wang, Xiao He, Shengshan Hou, Wenkai Feng, and Changjiang Liu

Experimental study of the shear strength criterion of rock structural plane based on threedimensional surface description

https://doi.org/10.1515/rams-2022-0045 received December 11, 2021; accepted June 14, 2022

Abstract: The failure of rock mass is mainly due to the failure of the structural plane, which is an important factor to reduce the mechanical properties and stability of rock mass. The shear strength of rock mass is one of the parameters for the stability calculation of large-scale rock mass engineering. The shear strength of a rock structural plane is strongly influenced by surface morphology. Considerable research has been conducted regarding the correlation between two-dimensional structural plane morphology and shear strength. However, quantitative research on three-dimensional (3D) morphology is relatively limited. In this study, 3D printing technology was used to create molds. Using cement and sand as the main materials, additives such as early strength and waterreducing agents were added, and test samples of irregular surface topography were created. The 3D roughness was quantified by formula calculation. Using a ZScanner® 800 hand-held 3D laser scanner to perform scanning on the structural surface, the parameter curve was analysed by generating 3D coordinate information and a 3D image of the fracture surface, and the quantitative parameter M_n^{3D} describing the 3D morphology of the structural surface was constructed. The change rule of $R_{\rm p}^{\rm 3D}$ and joint roughness coefficient (JRC) were analysed under different scanning resolutions, $\Delta(r)$, the scanning precision was suggested, and the functional relationship between JRC and M_n^{3D} was established. Finally, a formula for shear strength parameters considering the 3D characteristics of a structural plane surface was established. The model validation results show that the experimental data were within the 95% confidence band of the model curve, the average error of the shear strength was 10.4%, the errors of friction angle and cohesion, C, were 3.4 and 9.4%, and the reliability was fine.

Keywords: structural plane, three-dimensional, topography, laser scanning, shear strength, roughness coefficient

List of symbols

cohesion of the material

ICS joint compression strength **IRC** joint roughness coefficient $M_{\rm p}^{\rm 3D}$ reciprocal of 3D fluctuation coefficient of the structural plane 3D fluctuation coefficient of the structural plane. S_{Q} area of the structural surface slope S_{T} area of the horizontal projection Δr scanning resolution axial stress confining pressure σ_3 normal stress $\sigma_{\rm n}$ peak shear strength $\tau_{
m p}$ internal friction angle of the material

basic friction angle of the structural plane

Civil Engineering, State Key Laboratory of Geohazard Prevention and Geoenvironment Protection, Chengdu University of Technology,

Chengdu 610059, China, e-mail: 65341207@qq.com

Feng Ji, Lei Wang, Xiao He, Wenkai Feng: School of Environment and Civil Engineering, State Key Laboratory of Geohazard Prevention and Geoenvironment Protection, Chengdu University of Technology, Chengdu 610059, China

* Corresponding author: Yuchuan Shi, School of Environment and

Shengshan Hou: Geological Disaster Technical Guidance Center of the Ministry of Natural Resources, China institute of Geo-Environment Monitoring, Beijing 100081, China

Changjiang Liu: School of Civil Engineering, Guangzhou University, Guangzhou, 510006, China

1 Introduction

There are a large number of joint planes in the natural rock mass, which significantly affect the mechanical properties of the rock mass [1–3]. The physical and mechanical properties of the joint plane in rock mass are a

 $\varphi_{\rm b}$

complex system with geometric space characteristics. The instability of rock mass engineering and the occurrence of geological disasters are mostly related to the weakening of the mechanical properties of rock mass [4]. By controlling the shear strength of the jointed rock mass, the roughness of the joint plane has become one of the important factors affecting the mechanical properties of the rock mass structural plane [5]. The influence of joint surface morphology on the rock's mechanical properties is notable. To eliminate or reduce the rock morphological effects, model tests have been widely used. In the study by Patton, by introducing a structural plane physical model, the effect of serrated structures on the shear strength is studied [6]. By analysis of a total of 136 natural rock joints, the index of joint roughness coefficient (JRC) was proposed by Barton and Choubey [7] to describe the roughness of rock surfaces. Since the 1970s, joint morphology and its effects on mechanics have become a hot topic [7-14].

To evaluate the quantitative characteristics of the structural surface, Li et al. [15] introduced a meshing method of Schmidt projection to calculate the fractal dimension for joint orientation for the first time. By introducing the minimum spacing/trace length value and fractal dimension, the corresponding fractal probability density function was derived. Wei et al. [16] used cumulative relative fluctuation amplitude and weighted average gradient to characterize the morphological characteristics of the joint profile, and the JRC calculation formula was put forward. The quantitative characterization of ten standard JRC curves has been analysed by many scholars [17-23], and a set of statistical formulas have been developed. Some roughness parameters, such as root mean square of the deviation [17-22], structural function [17,18,21], and roughness profile index [18-21,24], were often mentioned. By using a total station, Feng et al. [25] put forward a new way to describe non-contact fracture roughness. In the study by Morelli [26], a new index for describing the JRC was put forward. In addition, some scholars have found that self-affine fractal and multifractal natures exist in joint morphology [27–29]. By analysing ten standard JRC curves, the effect of fractal dimension on joint strength has been studied. It was noted by Grasselli [9] that the initial contact area was correlated with the damaged zone and the peak shear strength. There are many methods to study and determine the roughness of a structural plane, but how to apply it to the deformation and failure of rock mass and quantitatively combine the roughness with the failure strength of rock mass has become an important research direction.

In the study by Barton and Choubey [7], a formula for the peak shear strength that combines the IRC, normal stress, and mechanical properties was put forward. Zheng et al. [30] proposed a generalized three-dimensional (3D) fractal dimension, which can comprehensively characterize the roughness, undulation, and anisotropy of structural surface morphology, and established the mathematical expression of a generalized 3D fractal dimension. Taking the effect of the slippage resistance of convex teeth in the shear direction into account, Grasselli [9] used the morphological quantification of 3D joint surfaces and proposed a peak shear strength prediction model. Furthermore, considerable work in this field has also been done by other researchers [5,31–35]. The research on structural surfaces mentioned in the above literature mainly focuses on 2D morphology, and it is necessary to further develop the research on 3D models. Combining 3D scanning and direct shear technology, it is feasible to explore and establish the criterion of peak strength of a structural plane [36]. The computation of JRC is cumbersome and requires a lot of study. The 3D morphological characteristics or the anisotropy of joint surfaces are not reflected. As a quantitative model to describe the 3D surface morphology, the parameters in the Grasselli model are too complex.

In this study, via material preparation and the 3D printing (3DP) method, structural test samples of different topographies were developed. The ratio of slope area to horizontal projection area was used to reflect the fluctuation in the 3D structure. Then, the change rule of the fluctuation state of the structural surface under different scanning resolutions was analysed using the 3D laser scanning method. A function model of the 3D structural surface and shear strength was established, then the shear test was used for validation (Figure 1).

2 Materials and methods

2.1 Material preparation

To prepare a rock model, a mix proportion procedure was used. The ratio of cement to sand is 1:1.5, and the ratio of cement to water is 1:0.3. In addition, 10% silica powder, 15% silicon carbide, 1.5% water reducer, and 2% accelerator were used in the whole mixture [37–47]. In the test, 52.5R composite silicate cement and sand were the main ingredients, silica powder and silicon carbide were additives, and a small amount of early strength admixture. To test the compressive strength and shear strength of the

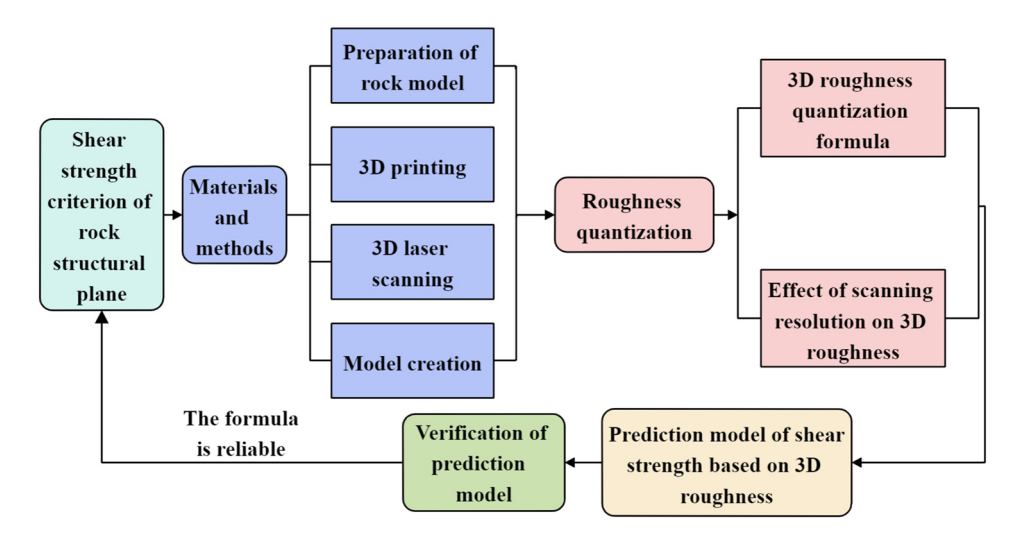


Figure 1: Flow chart of shear strength research of rock structural plane.

material, the dimensions and test standards of the modulus materials are shown in Table 1 (Figure 2).

2.2 3DP

3DP is a computer-controlled manufacturing technique that can fabricate objects with complicated geometry and internal structures repeatedly and accurately. Various printing techniques have been used to fabricate polymer composites. In this study, 3DP equipment and corresponding printing materials have been studied to produce molds of structural surface topography. Among the equipment, 3D printers using powder ink binders (PIB) are widely used. PIB printers are based on powder and liquid binders. Because PIB printers are made from sand powder, the resulting product may be more visually like rock material.

2.3 3D laser scanning

Hand-held 3D laser scanners are used to measure structural surface topography as they have high scanning speed and high precision. In this study, a ZScanner®

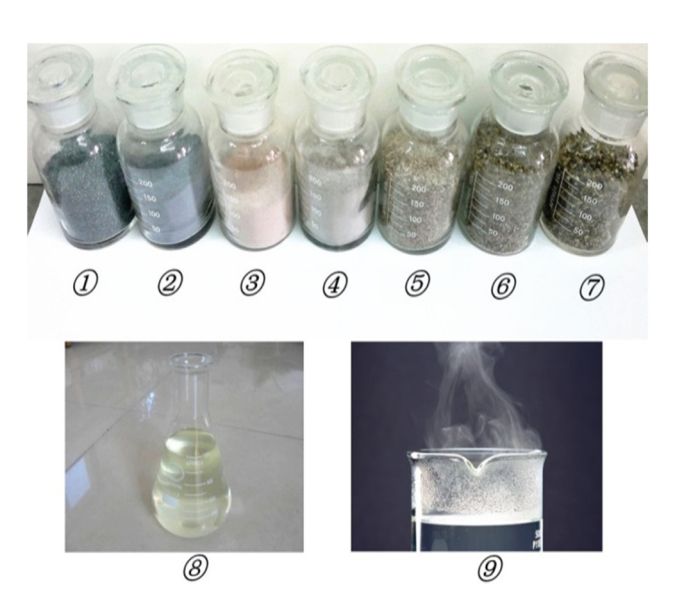


Figure 2: Components of similar raw materials. ① Green SiC,
② Micro silicon powder, ③ Early-strength admixture, ④ Portland cement, ⑤ Fine sand, ⑥ Coarse sand, ⑦ Aggregate (3-6 mm),
⑥ Carboxylic water-reducer, and ⑨ Warm water (30-45°C).

800 handheld 3D laser scanner was used, in which the maximum scanning accuracy can reach 0.04 mm. The instrument is shown in Figure 3, and the process of obtaining the surface morphology of the structural plane

Table 1: Testing type, specimen dimensions, and standard use in testing

Testing item	Sample size	Standard
Comprehensive strength Tensile strength Shear strength	ϕ 50 mm × 100 mm ϕ 50 mm × 50 mm 100 mm × 100 mm × 100 mm	American Society for Testing Material International Society for Rock Mechanics



Figure 3: ZScanner® 800 hand-held 3D laser scanner.

is shown in Figure 4, which included instrument installation, scanning specimen preparation, pasting the sensitive plate, open scanning of software, adjusting the laser power and other configurations, scanning the specimen, saving the file, data processing, model reconstruction, and the analysis result. After the scan is completed, a coordinate transformation of the data is required. *Geomagic Qualifier & Studio* can quickly complete the transformation of coordinates. The principle of transformation can be expressed as Formula 1 as follows:

$$\begin{bmatrix} X \\ Y \\ Z \end{bmatrix} = R(\partial, \beta, \gamma) \begin{bmatrix} X \\ Y \\ Z \end{bmatrix} + \begin{bmatrix} X_0 \\ Y_0 \\ Z_0 \end{bmatrix}, \tag{1}$$

where $R(\partial, \beta, \gamma)$ represents the rotating vector and $[x_0, y_0, z_0]^T$ represents the transformation vector between different coordinate systems.

2.4 Model creation

In this study, a 3D zigzag structural plane was processed. The model size was $10~\text{cm}\times 10~\text{cm}\times 5~\text{cm}$. The geometric

features of the convex teeth were controlled by the fluctuation angle (i) and the fluctuation height (h). Six serrated models were created, and their dimensions were $i = 60^{\circ}$, $h = 1 \, \text{cm}$; $i = 45^{\circ}$, $h = 1 \, \text{cm}$; $i = 30^{\circ}$, $h = 1 \, \text{cm}$; $i = 60^{\circ}$, $h = 0.5 \, \text{cm}$; $i = 45^{\circ}$, $h = 0.5 \, \text{cm}$; and $i = 30^{\circ}$, $h = 0.5 \, \text{cm}$, as shown in Figure 5.

3 Roughness quantization of the 3D surface of the structural surface

3.1 3D roughness quantization formula

Figure 6 shows a normal four-pyramid model; point O is the projection of point E on the plane ABCD. Line EF is the section line of the model. By cutting the convex teeth along the line EF, the roughness profile can be obtained. The profile roughness coefficient R_{pl} is used to represent the fluctuation of the structural plane. $R_{pl} = \text{EF/OF}$, and its coordinate expression is as follows:

$$R_{p1} = \frac{[(y_3 - y_1)^2 + (z_2 - z_1)^2]^{1/2}}{y_3 - y_1}.$$
 (2)

Triangle \triangle ABE and triangle \triangle AOB have a public side AB, EF \perp AB, and OF \perp AB, and \triangle ABE is a projection of the ABCD in plane \triangle AOB, S_{\triangle ABE} = $\frac{1}{2}$ (AB \times EF), S_{\triangle AOB = $\frac{1}{2}$ (AB \times OF).

$$\frac{S\Delta ABE}{S\Delta AOB} = \frac{1/2(AB \times EF)}{1/2(AB \times OF)} = \frac{EF}{OF},$$

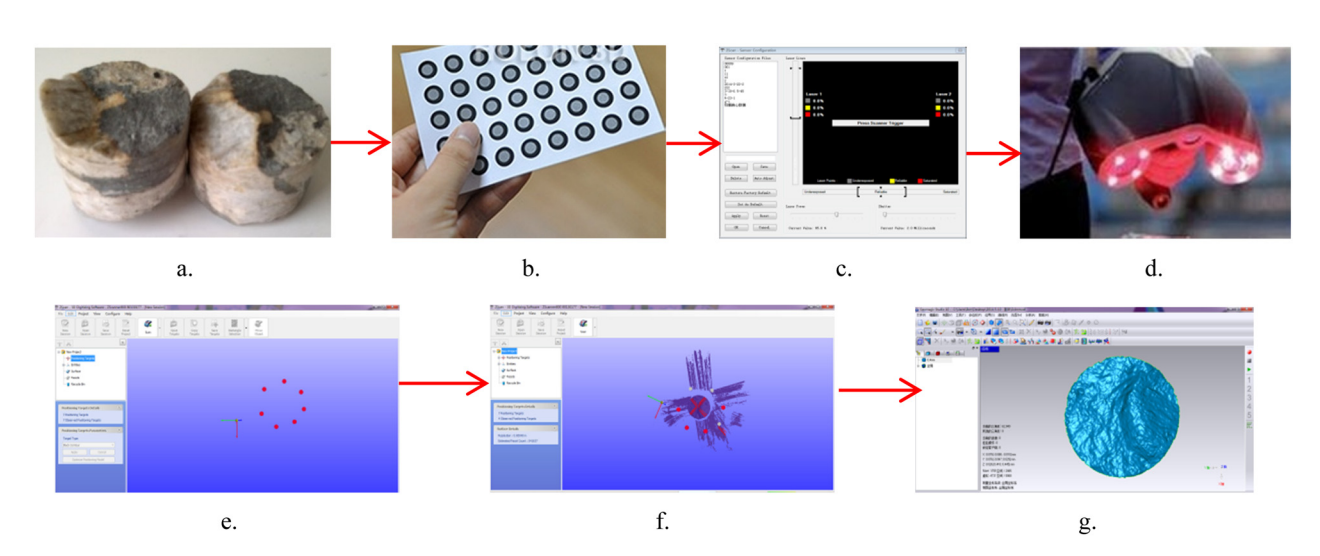


Figure 4: 3D laser scanning process. (a) Scanning specimen preparation. (b) Paste the sensitive plate. (c) Debug scanner. (d) Prescan. (e) Scan sensitive plate. (f) Scan structural plane. (g) Data processing.

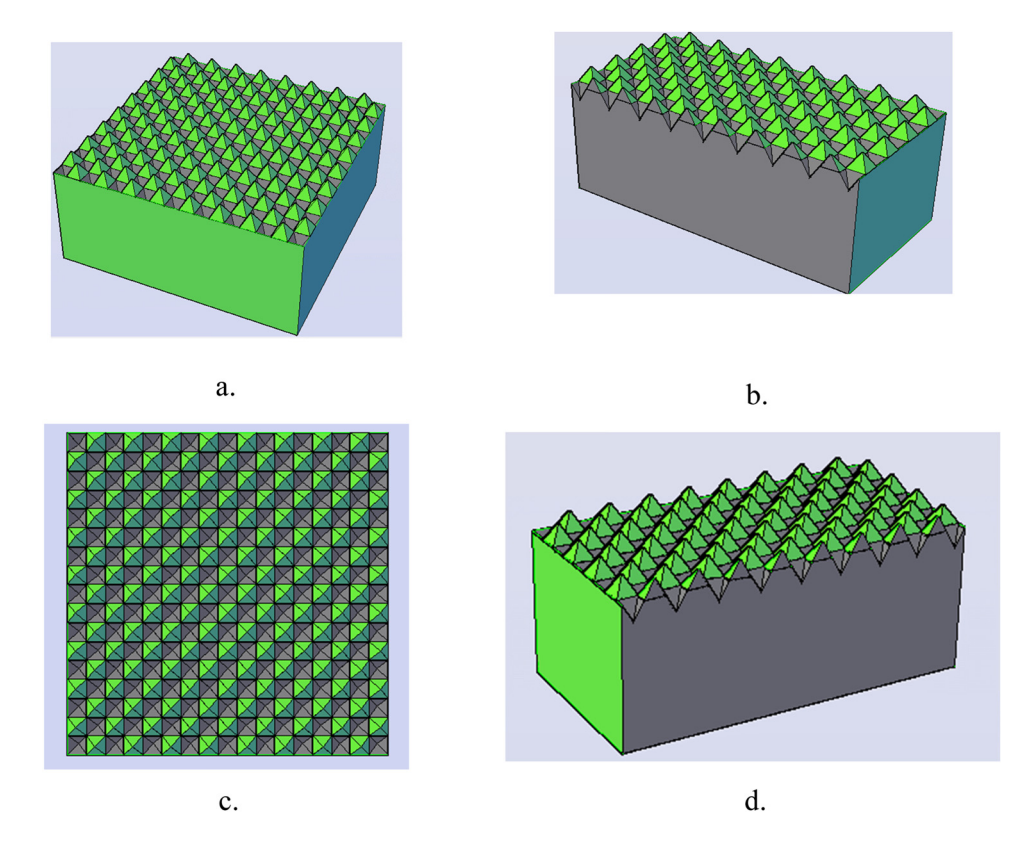


Figure 5: 3D zigzag model. (a) Model side view. (b) Transverse cutting view. (c) Model bird's-eye view. (d) Longitudinal cutting view.

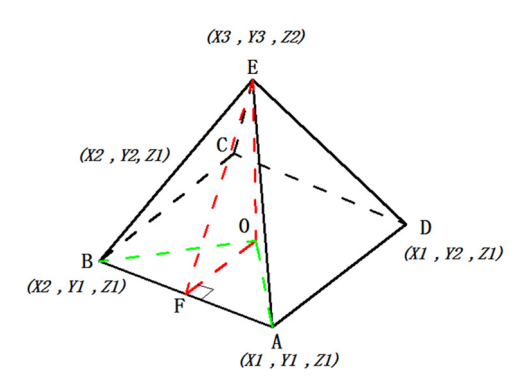


Figure 6: Normal four-pyramid model and coordinates.

$$\frac{\text{EF}}{\text{OF}} = R_{p1} = \frac{[(y_3 - y_1)^2 + (z_2 - z_1)^2]^{1/2}}{y_3 - y_1}.$$

Thus, we obtain formula (3) as follows:

$$\frac{S\Delta ABE}{S\Delta AOB} = R_{p1} = \frac{[(y_3 - y_1)^2 + (z_2 - z_1)^2]^{1/2}}{y_3 - y_1}.$$
 (3)

The profile roughness coefficient of the 3D surface of the structural surface is denoted by R_p^{3D} . Equation 4 can be used to describe the entire structural plane as follows:

$$R_{\rm p}^{3D} = \frac{\sum_{i=1}^{N-1} S_{\rm Q}_i}{\sum_{i=1}^{N-1} S_{\rm T}_i} = \frac{S_{\rm Q}}{S_{\rm T}},\tag{4}$$

where S_Q represents the slope area of the structural plane and S_T represents the projected area in the horizontal plane.

The profile roughness coefficient $R_{\rm p}$ can reflect the undulating state of the structure. However, to avoid the surface area of the structural surface becoming 0, the situation of $R_{\rm p}^{\rm 3D}$ tends to infinity. The reciprocal $M_{\rm P}$ of the profile roughness coefficient $R_{\rm p}$ is adopted, and the expression of $M_{\rm p}$ is as follows:

$$M_{\rm p} = \left\{ \sum_{i=1}^{N-1} \frac{\left[(y_3 - y_1)^2 + (z_2 - z_1)^2 \right]^{1/2}}{y_3 - y_1} \right\}^{-1}.$$
 (5)

3.2 Effect of scanning resolution on 3D roughness

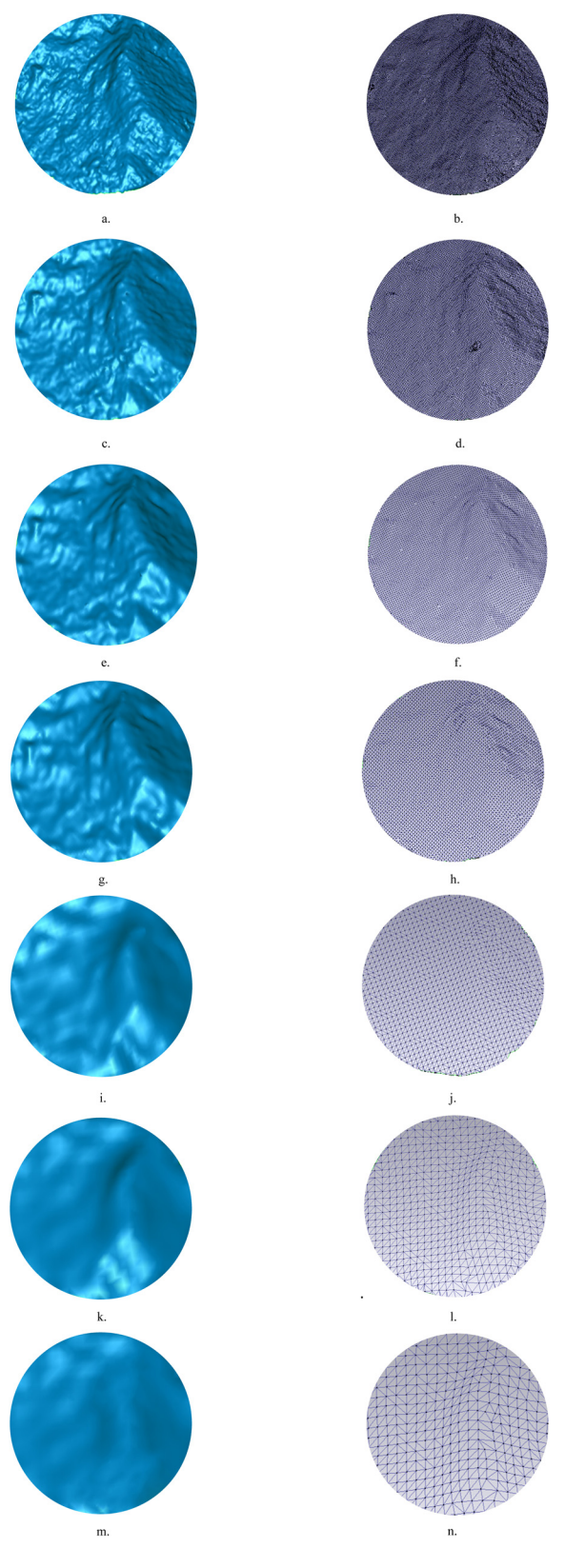
In general, the higher the resolution, the more detailed the model is, and the closer it is to the real shape of the structural plane. To study the effect of scanning accuracy on the 3D roughness coefficient $R_{\rm p}^{\rm 3D}$, different scanning resolutions were used to scan the structural surface topography to explore the relationship between Δr and $R_{\rm p}^{\rm 3D}$. The resolution of the scanning instrument was 0.4, 0.6, 0.8, 1.0, 2.0, 3.0, and 4.0 mm, respectively, and 3D data of the structural surface were obtained. Then, the data were imported into the ploy-works 8.0 reconstruction software to process, generate 3D images of the structural surface, and develop statistics on the related geometric parameters. The 3D scanning model and grid are shown in Figure 7. The geometric parameters of the structural plane are shown in Table 2.

Table 2 shows, when the resolution of $\Delta r = 0.4$ mm, the scanning model is most similar to that of the original rock surface, and the detailed characteristics are very clear. When the resolution is gradually reduced, the details of the structural surface become blurred, and the model surface becomes smooth. When the resolution reaches 4 mm, the detailed morphology can hardly be observed, and only the areas with prominent fluctuations can be reflected; the whole plane gradually tends to a smooth plane. The relationship between scanning resolution and R_p^{3D} is shown in Figure 8. With a decrease in scanning resolution (Δr increasing), R_p^{3D} gradually decreases, representing a power index relationship.

The JRC value is the parameter reflecting the roughness of the structural surface. At different resolutions, the roughness coefficient JRC of the structural surface image changes. To study the change rule of JRC under different scanning accuracies, six profile lines were taken of the different scanning resolution models. Based on the Barton model, which links the roughness of the structural plane with the shear strength and compressive strength, the roughness coefficient JRC value of the profile line was calculated. The relationship between Δr and JRC was studied. Similar to Figure 9, the JRC values of the profile lines are shown in Figure 10.

The relationship curve of JRC to Δr is shown in Figure 11. With a decrease in resolution (Δr increasing), the roughness of the structural surface gradually decreases, and they are related exponentially. Its change trend is basically consistent with the change trend of $M_{\rm p}^{\rm 3D}$, and a relationship between $M_{\rm p}^{\rm 3D}$ and JRC is established as follows:

$$JRC = -444.52(R_p^{3D})^2 + 1050.8R_p^{3D} - 614.56.$$
 (6)



(caption on next page)

Figure 7: Model and grid of a 3D scanned model. (a) 3D model ($\Delta r = 0.4$ mm). (b) Triangular grid diagram ($\Delta r = 0.4$ mm). (c) 3D model ($\Delta r = 0.6$ mm). (d) Triangular grid diagram ($\Delta r = 0.6$ mm). (e) 3D model ($\Delta r = 0.8$ mm). (f) Triangular grid diagram ($\Delta r = 0.8$ mm). (g) 3D model ($\Delta r = 1.0$ mm). (h) Triangular grid diagram ($\Delta r = 1.0$ mm). (i) 3D model ($\Delta r = 2.0$ mm). (j) Triangular grid diagram ($\Delta r = 2.0$ mm). (k) 3D model ($\Delta r = 3.0$ mm). (l) Triangular grid diagram ($\Delta r = 3.0$ mm). (m) 3D model ($\Delta r = 4.0$ mm). (n) Triangular grid diagram ($\Delta r = 4.0$ mm).

We can see from the aforementioned figures that with a decrease in the scanning resolution (an increase in Δr), $R_p^{\rm 3D}$ and JRC gradually decrease. When the scanning resolution is reduced to 10.6 mm, the $R_p^{\rm 3D}$ value is 1.061. Substituting 10.6 into the formula in Figure 11, the JRC value is 0.01, which is near 0, indicating that the structural surface is near the plane. When the scanning resolution is enhanced, $R_p^{\rm 3D}$ and JRC also increase, but the JRC value does not increase when the scanning resolution reaches 0.2 mm. Therefore, we suggest that during the scanning process of the structural surface topography, the scanning resolution should be adjusted to be from 0.4 mm. At the same time, the function relationship between JRC and $M_p^{\rm 3D}$ was established, as shown in the following equation:

JRC =
$$-0.0028(M_p^{3D})^2 + 0.0098M_p^{3D} + 0.9076 (0.1 \text{ mm} < \Delta r < 1 \text{ mm}),$$
 (7)

where
$$M_p^{3D} = (R_p^{3D})^{-1} = \left(\frac{\sum_{i=1}^{N-1} S_{Qi}}{\sum_{i=1}^{N-1} S_{Ti}}\right)^{-1} = \left(\frac{S_Q}{S_T}\right)^{-1}$$
.

In the above formula, $M_{\rm p}^{\rm 3D}$ is the reciprocal of the undulation coefficient ($M_{\rm p}^{\rm 3D}=0$ represents the vertical horizontal plane, the projected area is 0, and $M_{\rm p}^{\rm 3D}=1$ indicates that the surface is near an ideal horizontal plane). $S_{\rm Q}$ represents the slope area of the structural surface. $S_{\rm T}$ represents the area of the horizontal projection. Δr is the scanning resolution (Figures 12 and 13).

4 Prediction model of shear strength based on 3D roughness

On the basis of the quantitative description of the 3D structural surface and the Barton model [48], we established a 3D shear strength estimation formula by adopting the $M_p^{\rm 3D}$ of the structural surface undulating coefficient a follows:

$$\begin{split} & \left[\tau = \sigma_{\rm n} t g \left[(-0.0028 (M_{\rm p}^{\rm 3D})^2 + 0.0098 M_{\rm p}^{\rm 3D} \ \, \sigma < 20 \text{ MPa,} \right. \right. \\ & \left. + 0.9076) l g \left(\frac{\rm JCS}{\sigma_n} \right) + \varphi_{\rm b} \right], \\ & \left[\tau = \sigma_{\rm n} t g \left[(-0.0028 (M_{\rm p}^{\rm 3D})^2 + 0.0098 M_{\rm p}^{\rm 3D} \ \, \sigma > 20 \text{ MPa.} \right. \right. \\ & \left. + 0.9076) l g \left(\frac{\sigma_1 - \sigma_3}{\sigma_n} \right) + \varphi_{\rm b} \right], \end{split}$$
(8)

 $(\Delta r = 0.4 \text{ mm})$, where

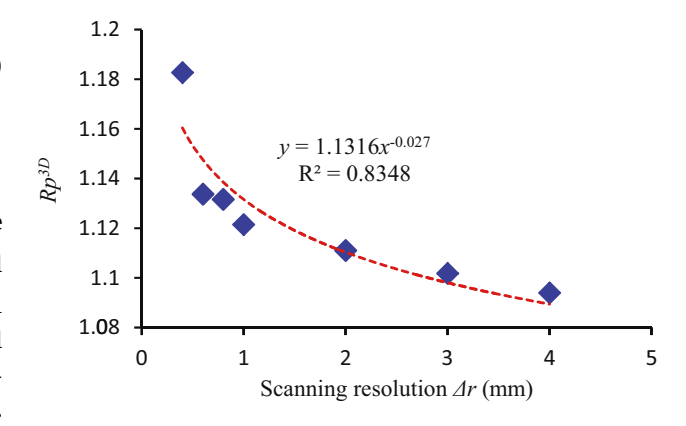


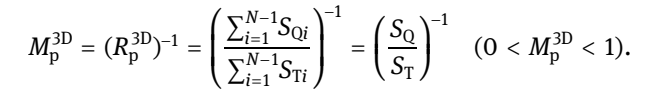
Figure 8: Relation curve of Δr with $R_{\rm p}^{\rm 3D}$.

Table 2: Geometric parameters of the structural plane at different resolutions

Number	Scanning resolution (mm)	Triangular mesh number	Slope area of the structural plane (mm²)	Area of the horizontal projection (mm²)	$R_{\rm p}^{\rm 3D}$	
1	0.4	62,040	5648.3	4775.94	1.182	
2	0.6	27,525	5414.6	4775.94	1.133	
3	0.8	15,650	5404.5	4775.94	1.131	
4	1	9,940	5356.1	4775.94	1.121	
5	2	2,620	5306.2	4775.94	1.111	
6	3	1,247	5262.2	4775.94	1.101	
7	4	706	5224.7	4775.94	1.093	



Figure 9: Section line of the structural plane.

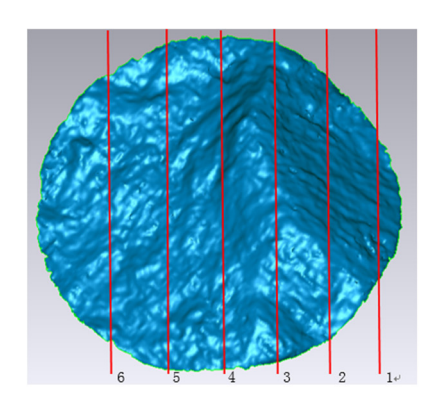


In the above formula, $M_{\rm p}^{\rm 3D}$ is the reciprocal of the undulation coefficient ($M_{\rm p}^{\rm 3D}=0$ represents the vertical horizontal plane, the projected area is 0, and $M_{\rm p}^{\rm 3D}=1$ indicates that the surface is near an ideal horizontal plane). $S_{\rm Q}$ represents the slope area of the structural surface. $S_{\rm T}$ represents the area of the horizontal projection. Δr is the scanning resolution. The joint compression strength (JCS) represents the compressive strength of the rock. $\varphi_{\rm b}$ is the basic friction angle of the structural plane.

5 Discussion

A shear test under different stress levels was conducted to verify the reliability of the shear strength model. The reliability of the theoretical formula was evaluated by comparing the error of the test value to the predicted value. During the experiment, the normal stress was 0.5, 1.0, 1.5, 2.0, 2.5, and 3.0 MPa. The structural surface sample is shown in Figure 14. The compressive strength was 52.5 MPa and the basic friction angle was 45.48° after 28 days of standard curing. The resolution of the scanning instrument was 0.4 mm, via scanning and calculation, $M_p^{\rm 3D} = 0.7642$.

Figure 15 shows the laser scanning image following the shear test under different stresses. With an increase in the normal stress, the loss degree of the structural surface gradually increases. When the normal stress is relatively low, the surface of the structural plane is significantly



damaged, and this results in a sliding type after climbing over the convex body.

$$\tau = \sigma \operatorname{tg} \varphi + C. \tag{9}$$

When the normal stress was increased gradually, the convex was cut and slippage shear failure occurred. According to the experimental data of the shearing results, the relationship curve between the shear stress and the positive stress was plotted. The shear stress was the vertical coordinate and the normal stress was the horizontal coordinate, and C and φ were obtained according to formula (9). At the same time, the theoretical prediction model was applied. C and φ were obtained after accurate determination of M_p^{3D} , JCS, and φ_b as shown in Figure 16.

Experimental values and theoretical prediction values were calculated, and the results are shown in Table 3. The friction angle was 41.5° and the cohesion coefficient *C* was 0.32 MPa by experiment. The friction angle was 42.9° and the cohesion *C* was 0.29 MPa using the theoretical prediction model. Through the linear fitting of the 95% confidence interval of the model formula, the experimental values are within the confidence band. The average error of the shear strength was 10.4%. The errors of friction angle and the cohesion *C* were 3.4% and 9.4%. The results show that the formula is reliable.

The test assumes that the structural plane is hard and does not consider the anisotropy of the structural plane. The established theoretical prediction model can well predict the friction angle and the cohesion C, but the shear strength is not very ideal when the normal stress is small. We believe that the cohesion C still has some internal relationships with $M_{\rm p}^{\rm 3D}$. Through the shear test of

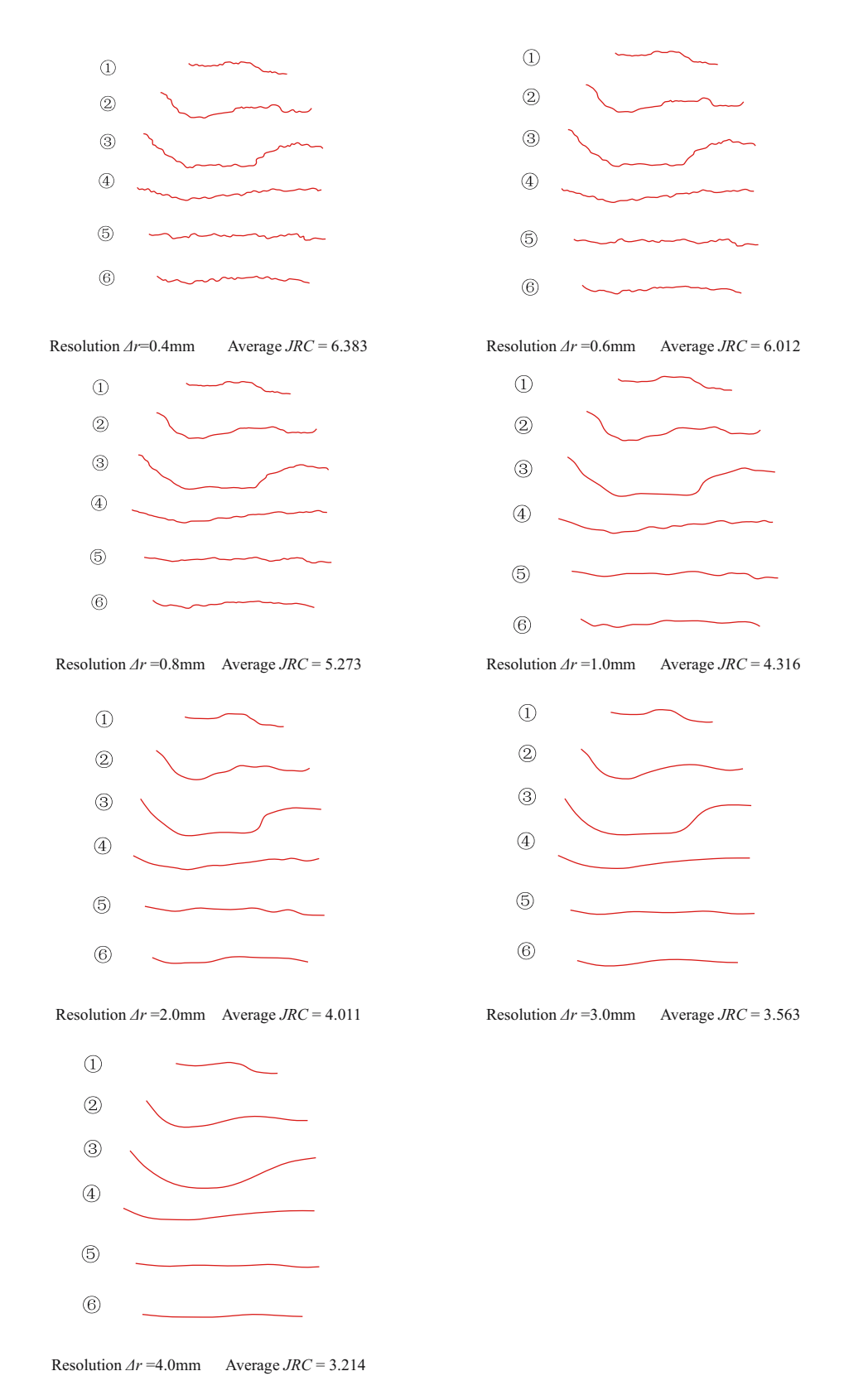


Figure 10: Sectional morphology and JRC value at different resolutions.

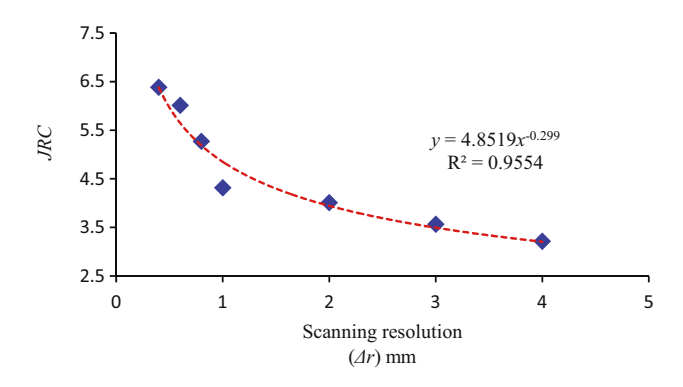


Figure 11: Relation curve of JRC with different resolutions.

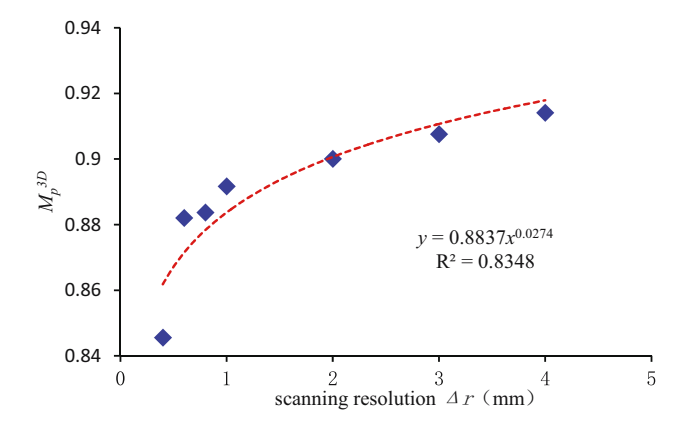


Figure 12: Relation curve of $M_p^{3D} - \Delta r$.

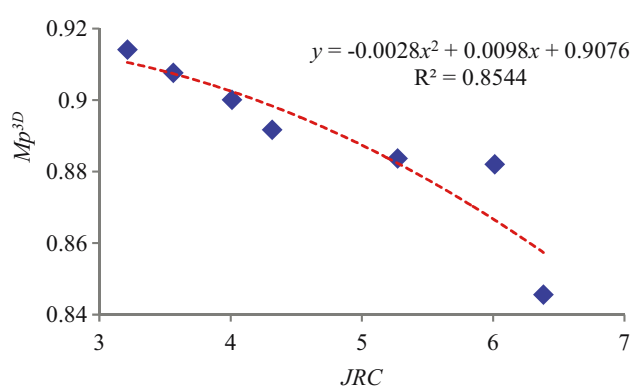


Figure 13: Relation curve of $M_{\rm D}^{\rm 3D}$ -JRC.

samples with different proportions, we may be able to find the relationship between them and then modify the theoretical model.

6 Conclusions

The model of an irregular structure was prepared via material preparation and 3DP. Laser scanning was used to obtain the surface topography of the rock structural surface and produce a quantitative model of the 3D topography of the irregular structure. Based on the fluctuation

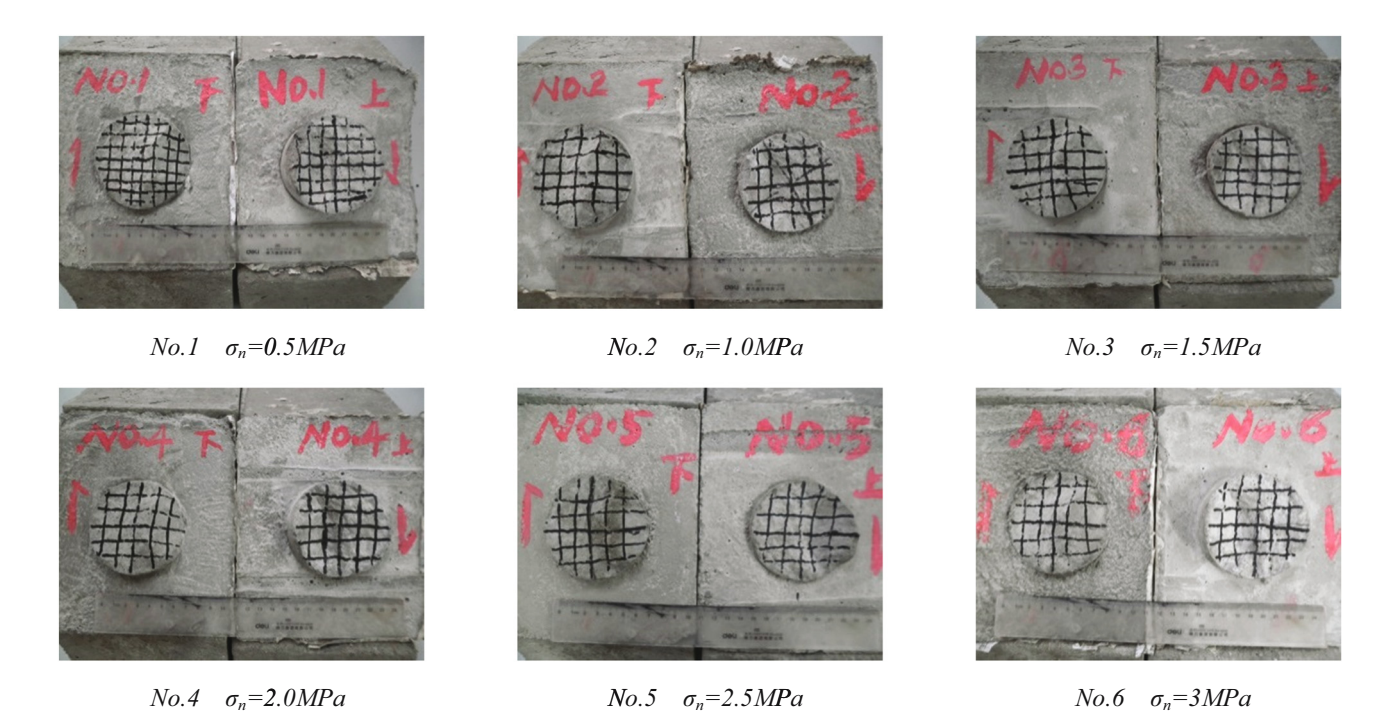


Figure 14: Model of structural plane sample.

3.0

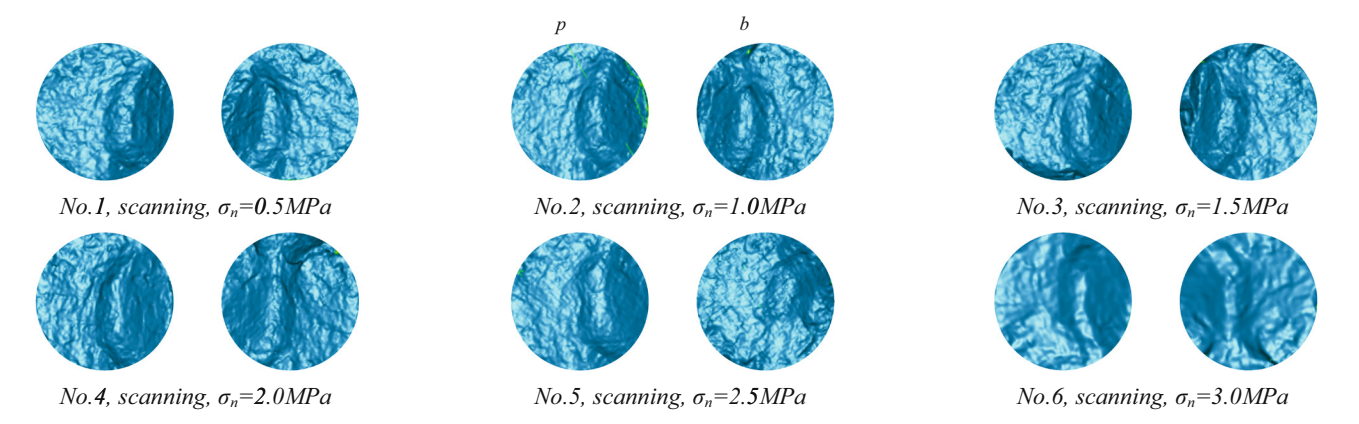


Figure 15: Laser scanning image of the structural plane after the shear test.

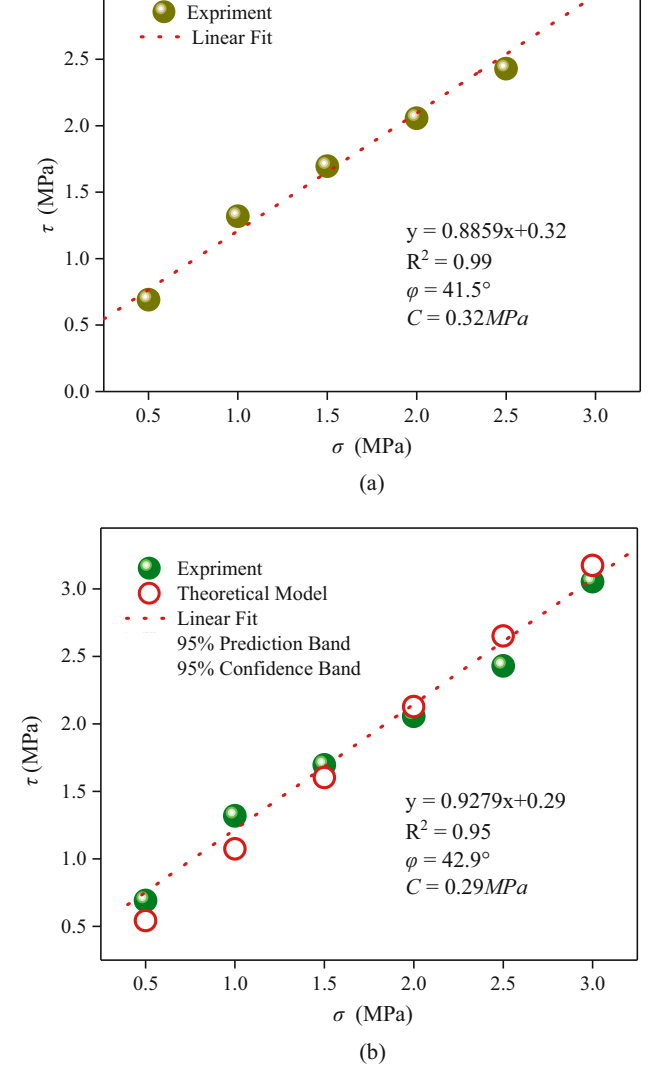


Figure 16: Relationship curves of τ - σ under different methods: (a) based on prediction model and (b) based on shear test.

coefficient $M_{\rm p}^{\rm 3D}$, the functional relationship between JRC and $M_{\rm p}^{\rm 3D}$ was established and embedded into the Barton model. Then, a prediction model was established for the shear strength, and the following was found:

- (1) Using the composite silicate cement and sand as main ingredients, silica powder and silicon carbide were added as additives, and with a small amount of early strength admixture, rock model materials were prepared. The ratio of cement to sand is 1:1.5, cement to water is 1:0.3. In addition, 10% silica powder, 15% silicon carbide, 1.5% water reducer, and 2% accelerator were used.
- (2) The undulation coefficient M_p^{3D} was used to describe the 3D fluctuation of the structural surface, and its value was the ratio of the slope area to the horizontal projection area for the structural surface.
- (3) A ZScanner[®] 800 portable 3D laser scanner was used for structural plane scanning, and the relationship curves of Δr to $M_{\rm p}^{\rm 3D}$ and JRC were obtained. With the decrease in resolution, the variation trend of JRC and $M_{\rm p}^{\rm 3D}$ decreases exponentially. The scanning resolution should be adjusted to be 0.4 mm during the scanning. The established functional relationship between JRC and $M_{\rm p}^{\rm 3D}$ is credible.
- (4) A formula for estimating the shear strength of the 3D structural surface was established based on the quantization parameters of the 3D structural surface. Experimental verification was conducted. The experimental values are within the confidence band of the 95% confidence interval of the model formula, and the average error of the shear strength was 10.4%. The errors of friction angle and the cohesion *C* were 3.4 and 9.4%, showing that the formula of the shear strength model is reliable.

	Table 3: Comparison of the exp	perimental value of shear strength	h and the prediction value of the theoretical model
--	--------------------------------	------------------------------------	---

No.	Normal stress (MPa)	a) Shear strength based on t		on tests	<i>M</i> _p ^{3D}	Shear strength based on prediction model			Error (%)
		τ (MPa)	C (MPa)	φ	_	τ (MPa)	C (MPa)	φ	_
1	0.5	0.6908	0.32	41.5	0.7642	0.5423	0.29	42.9	21.5
2	1.0	1.3188			0.7642	1.0742			18.6
3	1.5	1.6956			0.7642	1.6022			5.5
4	2.0	2.0560			0.7642	2.1277			3.4
5	2.5	2.4288			0.7642	2.6515			9.2
6	3.0	3.0533			0.7642	3.1737			4.0

Acknowledgments: We acknowledge the support of the National Key Research and Development Program of China (Grant No. 2021YFB2301304) and the Natural Science Foundation of China (No. 41977237). The authors are grateful to all the technicians who worked in the laboratory at SKLGP for aiding throughout the experimental work.

Funding information: The National Key Research and Development Program of China (Grant No. 2021YFB2301304) and the Natural Science Foundation of China (No. 41977237).

Author contributions: Feng Ji and Yuchuan Shi contributed to the conception of the study and field survey; Lei Wang and Xiao He performed the experiment; Shengshan Hou and Wenkai Feng contributed significantly to analysis and manuscript preparation; Feng Ji and Lei Wang performed the data analyses and wrote the manuscript; Shengshan Hou, Wenkai Feng and Changjiang Liu helped perform the analysis with constructive discussions.

Conflict of interest: Authors state no conflict of interest.

Data availability statement: All data included in this study are available upon request by contact with the corresponding author.

References

- [1] Yao, C., Q. Jiang, J. Shao, and C. Zhou. Modelling of hydro-mechanical coupling and transport in densely fractured rock mass. *European Journal of Environmental and Civil Engineering*, Vol. 19, No. 5, 2013, pp. 521–538.
- [2] Yao, C., Q. H. Jiang, and J. F. Shao. Numerical simulation of damage and failure in brittle rocks using a modified rigid block spring method. *Computers and Geotechnics*, Vol. 64, 2015, pp. 48-60.
- [3] Jiang, Q., W. Wei, N. Xie, and C. Zhou. Stability analysis and treatment of a reservoir landslide under impounding

- conditions: A case study. *Environmental Earth Sciences*, Vol. 75, No. 1, 2015.
- [4] Zhou, Y. Q., Q. Sheng, N. N. Li, and X. D. Fu. The dynamic mechanical properties of a hard rock under true triaxial damage-controlled dynamic cyclic loading with different loading rates: A case study. *Rock Mechanics and Rock Engineering*, Vol. 55, 2022, pp. 2471–2492. doi: 10.1007/ s00603-021-02756-w.
- [5] Zhang, X., Q. Jiang, N. Chen, W. Wei, and X. Feng. Laboratory investigation on shear behavior of rock joints and a new peak shear strength criterion. *Rock Mechanics and Rock Engineering*, Vol. 49, No. 9, 2016, pp. 3495–3512.
- [6] Patton, F. D. Multiple modes of shear failure in rock. Proceeding of the Congress of International Society of Rock Mechanics, 1966, pp. 509-513.
- [7] Barton, N. and V. Choubey. The shear strength of rock joints in theory and practice. Rock Mechanics Felsmechanik Mécanique des Roches, Vol. 10, No. 1, 1977, pp. 1–54.
- [8] Barton, N. Review of a new shear-strength criterion for rock joints. *Engineering Geology*, Vol. 7, No. 4, 1977, pp. 287–332.
- [9] Grasselli, G. Shear Strength of Rock Joints Based on Quantified Surface Description. Doctoral dissertation. Federal Institute of Technology, Swiss, 2001.
- [10] Asadollahi, P. and F. Tonon. Constitutive model for rock fractures: Revisiting Barton's empirical model. *Engineering Geology*, Vol. 113, No. 1–4, 2010, pp. 11–32.
- [11] Bahaaddini, M., P. C. Hagan, R. Mitra, and B. K. Hebblewhite. Scale effect on the shear behaviour of rock joints based on a numerical study. *Engineering Geology*, Vol. 181, No. 1, 2014, pp. 212–233.
- [12] Bahaaddini, M., P. C. Hagan, R. Mitra, and M. H. Khosravi. Experimental and numerical study of asperity degradation in the direct shear test. *Engineering Geology*, Vol. 204, No. 8, 2016, pp. 41–52.
- [13] Ji, F., C. J. Liu, Y. Zhang, L. B. Zheng, K. Pan, and X. Tan. Highstrength model material production for structural plane replica and its shear testing. *KSCE Journal of Civil Engineering*, Vol. 22, No. 1, 2017, pp. 174–184.
- [14] Singh, H. K. and A. Basu. Shear behaviors of 'real' natural unmatching joints of granite with equivalent joint roughness coefficients. *Engineering Geology*, Vol. 21123, 2016, pp. 120–134.
- [15] Li, L., W. Wu, M. H. El Naggar, G. Mei, and R. Liang. Characterization of a jointed rock mass based on fractal geometry theory. *Bulletin of Engineering Geology and the Environment*, Vol. 78, No. 8, 2019, pp. 6101–6110.

- [16] Wei, Y., L. Sifan, T. Hanhua, N. Jiandong, J. Zhiling, L. Xilai, et al. A new approach for quantifying the two-dimensional joint roughness coefficient (JRC) of rock joints. *Environmental Earth Sciences*, Vol. 80, 2021, id. 484.
- [17] Tse, R. and D. M. Cruden. Estimating joint roughness coefficients. *International Journal of Rock Mechanics and Mining Sciences*, Vol. 16, No. 5, 1979, pp. 303–307.
- [18] Yu, X. and B. Vayssade. Joint profiles and their roughness parameters. *International Journal of Rock Mechanics and Mining Sciences and Geomechanics Abstracts*, Vol. 28, No. 4, 1991, pp. 333–336.
- [19] Yang, Z. Y., S. C. Lo, and C. C. Di. Reassessing the joint roughness coefficient (JRC) estimation using Z2. *Rock Mechanics and Rock Engineering*, Vol. 34, No. 3, 2001, pp. 243–251.
- [20] Tatone, B. S. A. and G. Grasselli. A new 2D discontinuity roughness parameter and its correlation with JRC. *International Journal of Rock Mechanics and Mining Sciences*, Vol. 47, No. 8, 2010, pp. 1391–1400.
- [21] Jang, H. S., S. S. Kang, and B. A. Jang. Determination of joint roughness coefficients using roughness parameters. *Rock Mechanics and Rock Engineering*, Vol. 47, No. 6, 2014, pp. 2061–2073.
- [22] Li, Y. and Y. Zhang. Quantitative estimation of joint roughness coefficient using statistical parameters. *International Journal* of Rock Mechanics and Mining Sciences, Vol. 77, 2015, pp. 27–35.
- [23] Liu, X. G., W. C. Zhu, Q. L. Yu, S. J. Chen, and R. F. Li. Estimation of the joint roughness coefficient of rock joints by consideration of two-order asperity and its application in double-joint shear tests. *Engineering Geology*, Vol. 220, 2017, pp. 243–255.
- [24] Abolfazli, M. and A. Fahimifar. An investigation on the correlation between the joint roughness coefficient (JRC) and joint roughness parameters. *Construction and Building Materials*, Vol. 25911, 2020, id. 120415.
- [25] Feng, Q. H., N. Fardin, L. Jing, and O. Stephansson. A new method for in situ non-contact roughness measurement of large rock fracture surfaces. Rock Mechanics and Rock Engineering, Vol. 36, No. 1, 2003, pp. 3–25.
- [26] Morelli, G. L. On joint roughness: Measurements and use in rock mass characterization. *Geotechnical and Geological Engineering*, Vol. 32, No. 2, 2014, pp. 345–362.
- [27] Sakellariou, M., B. Nakos, and C. Mitsakaki. On the fractal character of rock surfaces. *International Journal of Rock Mechanics and Mining Sciences and Geomechanics Abstracts*, Vol. 28, No. 6, 1991, pp. 527-533.
- [28] Xie, H., J. A. Wang, and M. A. Kwaśniewski. Multifractal characterization of rock fracture surfaces. *International Journal of Rock Mechanics and Mining Sciences*, Vol. 36, No. 1, 1999, pp. 19–27.
- [29] Stach, S., J. Cybo, and J. Chmiela. Fracture surface fractal or multifractal. *Materials Characterization*, Vol. 46, No. 2, 2001, pp. 163–167.
- [30] Zheng, B., S. Qi, G. Luo, F. Liu, X. Huang, and S. Guo. Characterization of discontinuity surface morphology based on 3D fractal dimension by integrating laser scanning with ArcGIS. *Bulletin of Engineering Geology and the Environment*, Vol. 80, No. 3, 2021, pp. 2261–2281.

- [31] Son, B. K., Y. K. Lee, and C. I. Lee. Elasto-plastic simulation of a direct shear test on rough rock joints. *International Journal of Rock Mechanics and Mining Sciences*, Vol. 41, No. 3, 2004, pp. 354–359.
- [32] Singh, M. and K. S. Rao. Empirical methods to estimate the strength of jointed rock masses. *Engineering Geology*, Vol. 77, No. 1-2, 2005, pp. 127-137.
- [33] Usefzadeh, A., H. Yousefzadeh, H. Salari-Rad, and M. Sharifzadeh. Empirical and mathematical formulation of the shear behavior of rock joints. *Engineering Geology*, Vol. 164, No. 1–2, 2013, pp. 243–252.
- [34] Sun, F. C., C. X. She, L. T. Wan., and Q. R. Jiang. Peak shear strength criterion for rock joints based on three-dimensional morphology characteristics. *Chinese Journal of Geotechnical Engineering*, Vol. 36, No. 3, 2014, pp. 529–553.
- [35] Yang, J., G. Rong, D. Hou, J. Peng, and C. B. Zhou. Experimental study on peak shear strength criterion for rock joints. *Rock Mechanics and Rock Engineering*, Vol. 49, No. 3, 2016, pp. 821–835.
- [36] Liu, Q. S., Y. C. Tian, P. Q. Ji, and H. Ma. Experimental investigation of the peak shear strength criterion based on three-dimensional surface description. *Rock Mechanics and Rock Engineering*, Vol. 51, No. 4, 2017, pp. 1005–1025.
- [37] Liu, C. J., X. C. Huang, Y. Y. Wu, X. W. Deng, Z. L. Zheng, Z. Xu, et al. Advance on the dispersion treatment of graphene oxide and the graphene oxide modified cement-based materials. *Nanotechnology Reviews*, Vol. 10, No. 1, 2021, pp. 34–49.
- [38] Liu, C. J., X. Su, Y. Y. Wu, Z. L. Zheng, B. Yang, Y. B. Luo, et al. Effect of nano-silica as cementitious materials-reducing admixtures on the workability, mechanical properties and durability of concrete. *Nanotechnology Reviews*, Vol. 10, No. 1, 2021, pp. 1395–1409.
- [39] Xu, Z., Z. P. Huang, C. J. Liu, X. W. Deng, D. Hui, Y. T. Deng, et al. Experimental study on mechanical properties and microstructures of steel fiber-reinforced fly ash-metakaolin geopolymer-recycled concrete. *Reviews on Advanced Materials Science*, Vol. 60, No. 1, 2021, pp. 578–590.
- [40] Kim, S. H., S. M. Park, and S. J. Park. Role of dry ozonization of basalt fibers on interfacial properties and fracture toughness of epoxy matrix composites. *Nanotechnology reviews*, Vol. 10, No. 1, 2021, pp. 710–718.
- [41] Tang, Y. C., Z. Chen, W. H. Feng, Y. M. Nong, C. Li, and J. M. Chen. Combined effects of nano-silica and silica fume on the mechanical behavior of recycled aggregate concrete. *Nanotechnology Reviews*, Vol. 10, No. 1, 2021, pp. 819–838.
- [42] Ahmed, S., T. Meng, and M. Taha. Utilization of red mud for producing a high strength binder by composition optimization and nano strengthening. *Nanotechnology Reviews (Berlin)*, Vol. 9, No. 1, 2020, pp. 396–409.
- [43] Meng, T., K. J. Ying, X. F. Yang, and Y. P. Hong. Comparative study on mechanisms for improving mechanical properties and microstructure of cement paste modified by different types of nanomaterials. *Nanotechnology Reviews* (*Berlin*), Vol. 10, No. 1, 2021, pp. 370–384.
- [44] Zhuang, C. L. and Y. Chen. The effect of nano-SiO₂ on concrete properties: a review. *Nanotechnology Reviews (Berlin)*, Vol. 8, No. 1, 2019, pp. 562–572.

- [45] Long, Z., L. You, X. Tang, W. Ma, Y. Ding, and F. Xu. Analysis of interfacial adhesion properties of nano-silica modified asphalt mixtures using molecular dynamics simulation. *Construction* and Building Materials, Vol. 255, 2020, pp. 891–909.
- [46] Long, Z., S. Zhou, S. Jiang, W. Ma, Y. Ding, L. You, et al. Revealing compatibility mechanism of nanosilica in asphalt through molecular dynamics simulation. *Journal of Molecular Modeling*, Vol. 27, No. 3, 2021, pp. 27–81.
- [47] Long Z., X. Tang, N. Guo, Y. Ding, W. Ma, L. You, et al. Atomistic-scale investigation of self-healing mechanism in Nano-silica modified asphalt through molecular dynamics simulation. *Journal of Infrastructure Preservation and Resilience*, Vol. 3, No. 1, 2022, id. 4.
- [48] Barton, N. J. E. G. Review of a new shear-strength criterion for rock joints. *Engineering Geology*, Vol. 7, No. 4, 1973, pp. 287–332.